Virginia Commonwealth University
VCU Scholars Compass

Electrical and Computer Engineering Publications

Dept. of Electrical and Computer Engineering

2014

Excitonic recombination dynamics in non-polar GaN/AlGaN quantum wells

D. Rosales
Laboratoire Charles Coulomb, Universite Montepellier 2

B. Gil
Laboratoire Charles Coulomb, Universite Montepellier 2

T. Bretagnon
Laboratoire Charles Coulomb, Universite Montepellier 2

See next page for additional authors

Follow this and additional works at: http://scholarscompass.vcu.edu/egre_pubs

Part of the Electrical and Computer Engineering Commons

Rosales, D., Gil, B., & Bretagnon, T., et al. Excitonic recombination dynamics in non-polar GaN/AlGaN quantum wells. Journal of Applied Physics, 115, 073510 (2014). Copyright © 2014 AIP Publishing LLC.

Downloaded from

http://scholarscompass.vcu.edu/egre_pubs/194

This Article is brought to you for free and open access by the Dept. of Electrical and Computer Engineering at VCU Scholars Compass. It has been accepted for inclusion in Electrical and Computer Engineering Publications by an authorized administrator of VCU Scholars Compass. For more information, please contact libcompass@vcu.edu.

Authors
D. Rosales, B. Gil, T. Bretagnon, B. Guizal, F. Zhang, S. Okur, M. Monavarian, N. Izyumskaya, V. Avrutin, Ü Özgür, H. Morkoç, and J. H. Leach

This article is available at VCU Scholars Compass: http://scholarscompass.vcu.edu/egre_pubs/194

JOURNAL OF APPLIED PHYSICS **115**, 073510 (2014)

Excitonic recombination dynamics in non-polar GaN/AlGaN quantum wells

D. Rosales,[1,2] B. Gil,[1,2] T. Bretagnon,[1,2] B. Guizal,[1,2] F. Zhang,[3] S. Okur,[3] M. Monavarian,[3] N. Izyumskaya,[3] V. Avrutin,[3] Ü. Özgür,[3] H. Morkoç,[3] and J. H. Leach[4]
[1]*CNRS, Laboratoire Charles Coulomb, UMR 5221, F-34095 Montpellier, France*
[2]*Université Montpellier 2, Laboratoire Charles Coulomb, UMR 5221, F-34095 Montpellier, France*
[3]*Department of Electrical and Computer Engineering, Virginia Commonwealth University, Richmond, Virginia 23238, USA*
[4]*Kyma Technologies, Raleigh, North Carolina 27617, USA*

(Received 6 December 2013; accepted 4 February 2014; published online 21 February 2014)

The optical properties of $GaN/Al_{0.15}Ga_{0.85}N$ multiple quantum wells are examined in 8 K–300 K temperature range. Both polarized CW and time resolved temperature-dependent photoluminescence experiment are performed so that we can deduce the relative contributions of the non-radiative and radiative recombination processes. From the calculation of the proportion of the excitonic population having wave vector in the light cone, we can deduce the variation of the radiative decay time with temperature. We find part of the excitonic population to be localized in concert with the report of Corfdir *et al*. (Jpn. J. Appl. Phys., Part 2 **52**, 08JC01 (2013)) in case of *a*-plane quantum wells. © *2014 AIP Publishing LLC*. [http://dx.doi.org/10.1063/1.4865959]

I. INTRODUCTION

Nitride semiconductors have been running the show for more than quarter of a century after utilizing growth of high quality epilayers on foreign substrates. This is made possible by a thin low temperature and annealed buffer layer (either AlN, or GaN, or ternary alloys of multilayers).[1–4] which has been developed as a quality-impacting nucleation layer. The nucleation layer improved the material quality, reduced the residual n-type doping[3] and paved the way for demonstrations of p-doping,[5] blue light emitting diodes,[6] and nitride-based lasers.[7] As the high-quality samples became available on *c*-plane, as noted at Meijo University,[8] the deleterious effect of Quantum Confined Stark effect on light-matter interaction[9,10] and thus on performances of light-emitting diodes became evident.

The absence of the polarization fields normal to the QW plane in non-polar structures makes it possible to eliminate the excitation density dependence of the luminescence peak energy and variation of radiative lifetime with well thickness. Moreover, the eliminated separation of electrons and holes in non-polar QWs provides an ideal realm for studies of exciton recombination dynamics and excitonic recombination selection rules. So far, most of the studies in this field have focused on InGaN QWs widely utilized as active regions in blue/UV LEDs and laser diodes. It has been shown that, in this case, excitonic recombination dynamics are governed by localized states, rather than reflecting the intrinsic properties of the material.[11,12] Only few works so far have been dedicated to detailed investigation of excitonic recombination in non-polar GaN[13,14] and GaN/AlGaN QWs.[15] Therefore, it is imperative to study the optical anisotropy and exciton dynamics in non-polar GaN/AlGaN QWs.

Hetero-epitaxy along the non-polar[11,16,17] as well as semipolar orientations[18] was proposed as an alternative for producing improved nitride heterostructures and devices.[19] The lack of easily accessible bulk lattice matched substrates has hampered rapid progress but was a complementary source of motivation. To this end growth of bulk nitrides has been very limited although very actively pursued. The difficulty to grow large size high quality nitride boules is on its way to be overcome and a large variety of different growth approaches are now available either for growing bulk GaN or AlGaN or AlN.[20] Cutting these boules with chosen orientations and processing of the sawed surface to epiready standards is, however, a serious issue.

In this work, we examine the optical properties of GaN/AlGaN multiple quantum wells grown by metal–organic chemical vapor deposition (MOCVD) on free-standing bulk *m*-plane $(10\bar{1}0)$ GaN substrates. We first report the experimental anisotropy of the in plane optical response and followed by segueing into study of the properties of the excitonic emission. We find the excitonic recombination to be dominantly radiative up to about 80 K in our moderately shallow quantum wells. At higher temperatures, non-radiative recombination channels and the thermally induced de-trapping of the carriers photo-created in the barrier layers influence the recombination dynamics and the robustness of the photoluminescence. Following the experimental details, we analyze the optical anisotropy, photoluminescence intensity and decay times with varying temperature and close with concluding remarks.

II. EXPERIMENTAL DETAILS

Five 1.5 nm thick GaN quantum wells (QWs) separated by 8.5 nm $Al_{0.15}Ga_{0.85}N$ barrier layers were grown at a substrate temperature (Ts) of 1045 °C by MOCVD on free-standing bulk *m*-plane (10-10) GaN substrates provided by Kyma Technologies. Prior to QWs, a 400 μm GaN buffer was grown at Ts = 1050 °C followed by a 30 nm AlGaN layer. The multi-QW structure was capped with 20 nm AlGaN and 3 nm GaN. The schematic of the sample structure is shown in Figure 1.

The sample was mounted in a helium flow cryostat for all measurements and the temperature varied from 8 K to room temperature. The excitation was provided by a mode-locked frequency tripled titanium-sapphire laser, with a 2 ps

 © 2014 AIP Publishing LLC

[This article is copyrighted as indicated in the article. Reuse of AIP content is subject to the terms at: http://scitation.aip.org/termsconditions. Downloaded to] IP: 128.172.48.59 On: Mon, 19 Oct 2015 16:20:56

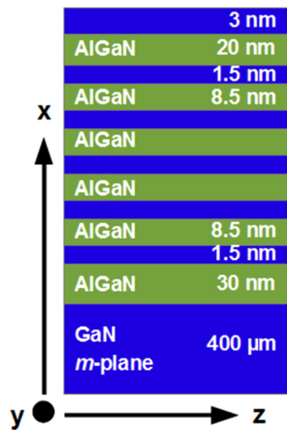

FIG. 1. Sketch of the sample design. Five periods of the quantum well basic building blocks are shown. The orientations of the x, y and z axes of the Cartesian basis are also indicated at the bottom corner on the left hand side of the figure.

pulse width and a wavelength of 266 nm. The focused laser spot diameter was 100 μm. We estimate that the photogenerated carrier density was about 3–4 $\times$ 10^{10} cm^{-2}. Due to the relatively slow photoluminescence decays, we have adapted a laser repetition rate of 4 MHz by using an acousto-optic modulator. The photoluminescence signal was dispersed by an imaging spectrometer and then temporally resolved by a streak camera with an overall time resolution of 8 ps.

III. OPTICAL ANISOTROPY AT LOW TEMPERATURE

It is well established, from group theory, that the optical response for the orientation under investigation, *m*-plane, is expected to be anisotropic in the growth plane. Experiments carried out on *a*-plane grown GaN/AlGaN non-polar quantum wells[21,22] have in particular reported it. Experiments recently published by Funato *et al*. on AlGaN/AlN *m*-plane grown quantum wells (here the quantum well layer is an aluminum-rich alloy) have also reported on optical anisotropy.[23] This is also confirmed by the data displayed in Figure 2 where a series of 8 K photoluminescence spectra recorded for various orientations of the electric field of the emitted photon radiation is plotted. We wish to emphasize the non-observation of photoemission in the 3.42 eV region. Such emission is typical for growth of non-polar GaN layers deposited on lattice mismatched foreign substrates[24] but is not observed for m-plane bulk GaN substrates. The signature of the bulk GaN photoluminescence (radiative recombination of donor-bound excitons at an energy peaking slightly below 3.480 eV at 8 K) is maximum when one probes the Γ_9 hole for the electric field of the emitted photon parallel to the $\vec{y}$ direction in the Cartesian basis. A 5 meV splitting is observed between the $\vec{y}$ and $\vec{z}$ polarizations, the latter being blue-shifted. At higher energies the inhomogeneously broadened photoluminescence band corresponding to radiative recombination of the confined excitons is noted at 3.616 eV with a full width at half maximum of 61 meV, while radiative recombination of excitons localized in the ternary barrier layers is observed at 3.709 eV with a full width at half maximum of 69 meV. From the energy of this recombination in the barrier layer and including the Stokes-shift always observed between the photoluminescence and a

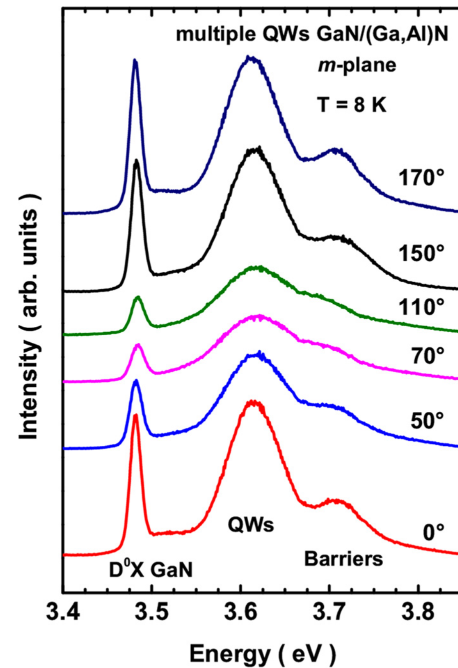

FIG. 2. Dependence of the photoluminescence intensity as a function of the orientation of the emitted photons. The origin of the angles is taken parallel to the $\vec{y}$ direction of the Cartesian basis.

photoreflectance or reflectance experiment,[25] we estimate the aluminum composition in the ternary barrier layers to be about 14%.[26] Figure 3 shows the intensities of the photoluminescence from the GaN, the multi-quantum well stack, and the barrier layers in polar coordinates. The crystallographic axes $(\vec{a}_1, \vec{a}_2, \vec{c})$, with respect to the unity vectors in the Cartesian basis $(\vec{x}, \vec{y}, \vec{z})$ are indicated on the schematic inserted at the right top corner of Figure 3. Interestingly, all three intensities display similar behavior versus the polarization angle. The degree of polarization $100 \times \frac{I_y - I_z}{I_y + I_z}$ (where I_u is the PL intensity recorded with electric field of the emitted photon parallel to the

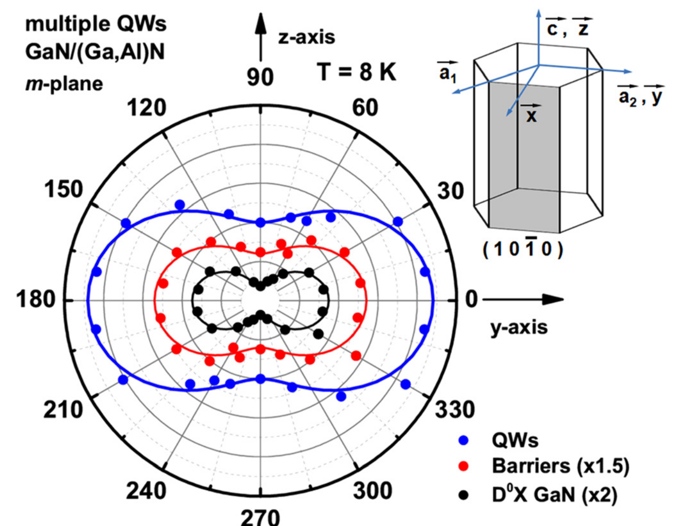

FIG. 3. Polar representation of the photoluminescence intensity for the MQWs stack (outer plot), for the barrier layers (middle plot) and for the GaN (inner plot). The orientation of the crystal is shown at the right hand top corner of the figure, to mark the orientations of the crystallographic axis $(\vec{a}_1, \vec{a}_2, \vec{c})$, with respect to the unity vectors of the Cartesian basis $(\vec{x}, \vec{y}, \vec{z})$.

[This article is copyrighted as indicated in the article. Reuse of AIP content is subject to the terms at: http://scitation.aip.org/termsconditions. Downloaded to] IP: 128.172.48.59 On: Mon, 19 Oct 2015 16:20:56

direction $\vec{u}$) for the quantum wells and barrier layers are similar, 38% for the quantum wells and 39% for the barrier layers. One also anticipates here that the crystal field splitting (which is known to change its sign from GaN to AlN) is still positive in these barrier layers under anisotropic tension. This argument is sustained by the high resolution of the photoluminescence spectra in the $\vec{E}//\vec{y}$ polarization compared to the spectra corresponding to photons collected with the $\vec{E}//\vec{z}$ polarization in our sample. Both the quantum wells and strained barrier layers are crystals with macroscopic C_{2v} orthorhombic symmetry. For the AlGaN barriers, it is the anisotropic strain (the degeneracy between $\vec{x}$ and $\vec{y}$ is lifted by strain) while for the multi-quantum well systems (MQWs), it is the breaking of translational symmetry in the $\vec{x}$ direction that reduces the symmetry. Following the work of Ref. 27, the compatibility relations between the two-fold representation of C_{6v} $\Gamma_5(\vec{x},\vec{y})$ and the irreducible representations of the abelian group C_{2v} are taken here as: $\Gamma_5(\vec{x},\vec{y}) = \Gamma_4'(\vec{x}) = \Gamma_2'(\vec{y})$

The theory predicts a short range spin exchange-related splitting between the Γ_1' and the Γ_2' excitons either for the quantum well or for the strained barrier layers. The inhomogeneous broadenings of the confined photoluminescence bands prevent the clear observation of splitting between the Γ_1' (allowed $\vec{E}//\vec{z}$) and Γ_2' (allowed $\vec{E}//\vec{y}$) excitons in the orthorhombic environments[23] as in our sample, even though the quantum confinement significantly enhances the short-range spin exchange interaction. Thus, to interpret the polarization signature of the photoluminescence intensity, we need to refer to the valence band structure and therefore work in the context of a band to band description of the recombination mechanisms which neglect the short range electron-hole spin exchange interaction but permits extraction of the physics of the light-matter interaction. The Γ_9 and Γ_7 representations of the C_{6v} double group are all transforming as Γ_5' in C_{2v} symmetry and one expects 3x3 matrix representations of the valence band physics.

Following the tradition, we treat the quantum confinement as a perturbation of the würtzite crystal and we express the wave function of the Γ_9 valence band in terms of the standard $|J, m_J\rangle$ notation $|\frac{3}{2}, \pm\frac{3}{2}\rangle = |1,\pm 1\rangle\begin{pmatrix}\uparrow\\ \downarrow\end{pmatrix} = \frac{x(\vec{r}) \pm iy(\vec{r})}{\sqrt{2}}\begin{pmatrix}\uparrow\\ \downarrow\end{pmatrix}$ where $x(\vec{r})$ and $y(\vec{r})$ are two of the p-type Bloch states in a spinless description and $\uparrow$ and $\downarrow$ represent the $^1/_2$ and $^{-1}/_2$ eigenstates of the spin operator. Concerning the Γ_7 valence bands we choose as wave function $|1,\mp 1\rangle\begin{pmatrix}\uparrow\\ \downarrow\end{pmatrix} = -\frac{x(\vec{r}) \mp iy(\vec{r})}{\sqrt{2}}\begin{pmatrix}\uparrow\\ \downarrow\end{pmatrix}$ and $|1,0\rangle\begin{pmatrix}\uparrow\\ \downarrow\end{pmatrix} = z(\vec{r})\begin{pmatrix}\uparrow\\ \downarrow\end{pmatrix}$. According to Park and Chuang[28] who performed in depth analysis of crystal orientation effects in würtzitic semiconductors, the 6x6 valence band Hamiltonian is obtained as two similar 3x3 Hamiltonians which we write as follows:

$$
\begin{array}{ccc}
\left|1,\pm 1\right\rangle\begin{pmatrix}\uparrow\\ \downarrow\end{pmatrix} & \left|1,\mp 1\right\rangle\begin{pmatrix}\uparrow\\ \downarrow\end{pmatrix} & \left|1,0\right\rangle\begin{pmatrix}\downarrow\\ \uparrow\end{pmatrix} \\
\Delta_1+\Delta_2+\frac{\hbar^2}{2m_0}(A_2+A_4)k_x^2 & -\frac{\hbar^2}{2m_0}A_5k_x^2 & 0 \\
-\frac{\hbar^2}{2m_0}A_5k_x^2 & \Delta_1-\Delta_2+\frac{\hbar^2}{2m_0}(A_2+A_4)k_x^2 & \sqrt{2}\Delta_3 \\
0 & \sqrt{2}\Delta_3 & \frac{\hbar^2}{2m_0}A_2k_x^2
\end{array}. \qquad (1)
$$

In this representation, Δ_1 depicts the matrix element which accounts for splitting of the p-type valence band states in a würtzitic environment, the convention is to express the operator as $\Delta_1 {L_z}^2$, where L_z is the z-component of the spinless hole angular momentum. The quantities Δ_2 and Δ_3 are the matrix elements required to describe the anisotropic spin orbit interaction. The quantities A_2, A_4, and A_5 are the Luttinger parameters that are introduced in the $\vec{k}\times\vec{p}$ description of the dispersion relation in the valence band of würtzitic semiconductors at Γ, m_0 represents the electron mass at rest, and k_x is the confined hole wave vector which takes discrete values thanks to the breaking of the translational symmetry in the $\vec{x}$ direction by alternating stacking of GaN and AlGaN layers [$(10\bar{1}0)$ growth plane]. We re-arrange Eq. (1) in the $x(\vec{r})$, $y(\vec{r})$ and $z(\vec{r})$ basis as:

$$
\begin{array}{ccc}
\vec{x}\begin{pmatrix}\uparrow\\ \downarrow\end{pmatrix} & \vec{y}\begin{pmatrix}\uparrow\\ \downarrow\end{pmatrix} & \vec{z}\begin{pmatrix}\downarrow\\ \uparrow\end{pmatrix} \\
\Delta_1+\frac{\hbar^2}{2m_0}(A_2+A_4)k_x^2+\frac{\hbar^2}{2m_0}A_5k_x^2 & i\Delta_2 & -\Delta_3 \\
-i\Delta_2 & \Delta_1+\frac{\hbar^2}{2m_0}(A_2+A_4)k_x^2-\frac{\hbar^2}{2m_0}A_5k_x^2 & -i\Delta_3 \\
-\Delta_3 & i\Delta_3 & \frac{\hbar^2}{2m_0}A_2k_x^2
\end{array}. \qquad (2)
$$

[This article is copyrighted as indicated in the article. Reuse of AIP content is subject to the terms at: http://scitation.aip.org/termsconditions. Downloaded to] IP: 128.172.48.59 On: Mon, 19 Oct 2015 16:20:56

From the form of the Hamiltonian and consistent with the expansions of the initial valence band basis in terms of $x(\vec{r})$, $y(\vec{r})$, and $z(\vec{r})$ p-type Bloch states, the eigenvectors of the problem can be written in the most generic way as:

$$\Psi(k_x) = \frac{a}{\sqrt{a^2+b^2+c^2}}x(\vec{r}) + \frac{b}{\sqrt{a^2+b^2+c^2}}y(\vec{r}) + \frac{c}{\sqrt{a^2+b^2+c^2}}z(\vec{r}), \quad (3)$$

with $a \neq b \neq c$, due the orthorhombic symmetry. Values of Δ_1, Δ_2, and Δ_3 are, respectively, 10.1 meV, 7.1 meV, and 5.5 meV for GaN.[29] Values of A_2, A_4, and A_5 are -0.53, -2.51, and -2.51, respectively.[30]

Plotted in Figure 4 is the dispersion of the eigenvalues in case of an infinitely deep GaN well for k_x values ranging between 0 and 1 nm^{-1}. We remark that starting from the Γ_9, Γ_7 and Γ_7 ordering for $k_x = 0$, increasing k_x produced a complex behavior with anti-crossings for high values of k_x to the relative ordering of the valence bands: *x*, *z*, and *y* (spin component is neglected since hole levels are all twice spin-degenerate). We remark that *y* and *z* states are nearly parallel to each other for high values of k_x. In terms of selection rules for the band to band transition the symmetry of the electric field of the photon may be $\Gamma_1^{'}$' ($\vec{E}//\vec{z}$), $\Gamma_2^{'}$ ($\vec{E}//\vec{y}$) or $\Gamma_4^{'}$ ($\vec{E}//\vec{x}$) in orthorhombic environment. Group theory indicates that non-vanishing matrix elements for the band-to-band transitions transform as z^2 or y^2 or x^2. In our experimental conditions, for photons collected with Poynting vectors parallel to $\vec{x}$ (light emitted through the *m*-plane surface), transitions can be recorded for $\Gamma_1^{'}$ ($\vec{E}//\vec{z}$) and $\Gamma_2^{'}$ ($\vec{E}//\vec{y}$) polarizations of the photon. Thus, transition between the confined electron state of the band and the *x*-type confined hole state should not be allowed in our experimental configuration. Our calculations indicate that the first dipole allowed transition is *z*-type

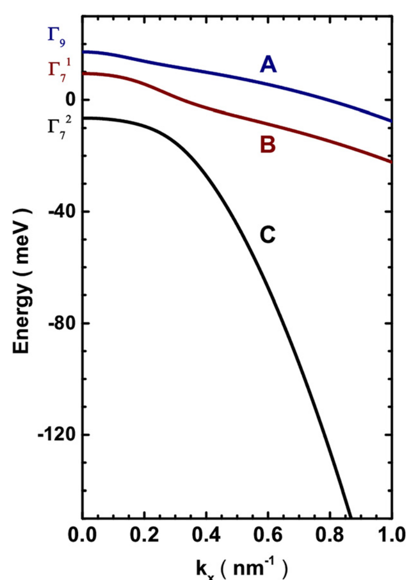

FIG. 4. Spectral dependence of the three valence band levels at $k_x \neq 0$ and $k_y = k_z = 0$. Note the initial anti-crossing of A and B levels at low values of k_x and the more pronounced one between B and C at higher values of k_x. For high k_x values levels A and B are quasi parallel and level C rapidly shifts a part the both of them.

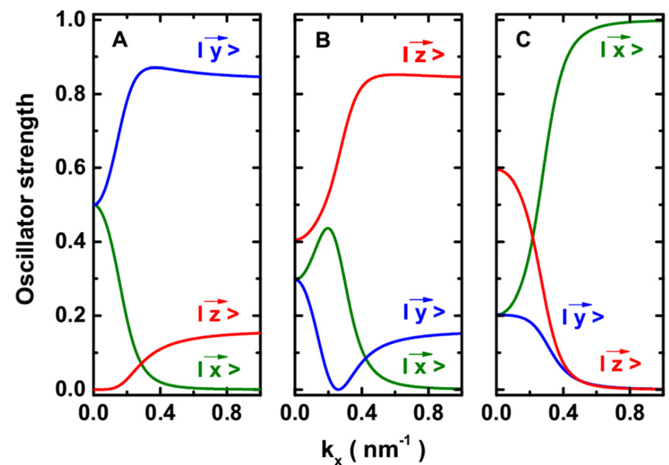

FIG. 5. Triptych representation of the expansion of A (left), B (middle), and C (right) levels against k_x. At high values of k_x, the ground state valence band (A) is dominantly built from $|\vec{y}\rangle$ Bloch state and from about 15 percents $|\vec{z}\rangle$ state. The second level (B) is dominantly built from $|\vec{z}\rangle$ Bloch state and from about 15 percents $|\vec{y}\rangle$ state. Note the quasi similar expansion of A and B through $|\vec{y}\rangle$ and $|\vec{z}\rangle$, respectively. Last for high values of k_x, it appears the C is built of $|\vec{x}\rangle$ Bloch state only. These expansions impact the selection rules for band to band transitions.

for high values of k_x (thin wells) and *y*-type for low values of k_x (wide wells). The oscillator strengths are obtained as the squared components of the coefficients of the eigenvectors projected over $\vec{z}$ and $\vec{y}$, respectively.

The modifications of the oscillator strengths for *z* (π_z), *y* (π_y), and *x* (π_x) polarization are plotted in Figure 5 for the three band to band transitions between the first confined electron states and the three confined valence bands. The amplitudes of the different transitions are obviously very different from what is expected in case of samples grown along the polar *c*-plane direction, but we remark that the lowest confined levels originating from the Γ_9 and the highest Γ_7 valence bands are both allowed in $\vec{E}//\vec{z}$ and $\vec{E}//\vec{y}$ polarizations. This qualitatively agrees with the theoretical prediction of Park.[31]

IV. TEMPERATURE DEPENDENT PHOTOLUMINESCENCE

Plotted in Figure 6 are photoluminescence spectra collected in the 8 K to 295 K range for $\vec{E}//\vec{y}$ and $\vec{E}//\vec{z}$ polarizations. A deconvolution procedure to fit the recombination lines of the photoluminescence was realized using a Gaussian function from the photoluminescence of the quantum well and the barrier layers. However, because of their overlapping nature and the similar behaviors of both polarizations, it is very difficult to discriminate between the contributions of the quantum wells and the barrier layers in the $\vec{E}//\vec{z}$ polarization. The photoluminescence intensities remain constant in the low temperature range up to typically 40–50 K and start to decrease with further increase in temperature.

In Figure 7, we plot the changes of the photoluminescence energy in the 8 K to 295 K temperature range for $\vec{E}//\vec{y}$ and $\vec{E}//\vec{z}$ polarizations. To a first extent, the luminescence for the quantum wells and barrier layers show fairly

[This article is copyrighted as indicated in the article. Reuse of AIP content is subject to the terms at: http://scitation.aip.org/termsconditions. Downloaded to] IP: 128.172.48.59 On: Mon, 19 Oct 2015 16:20:56

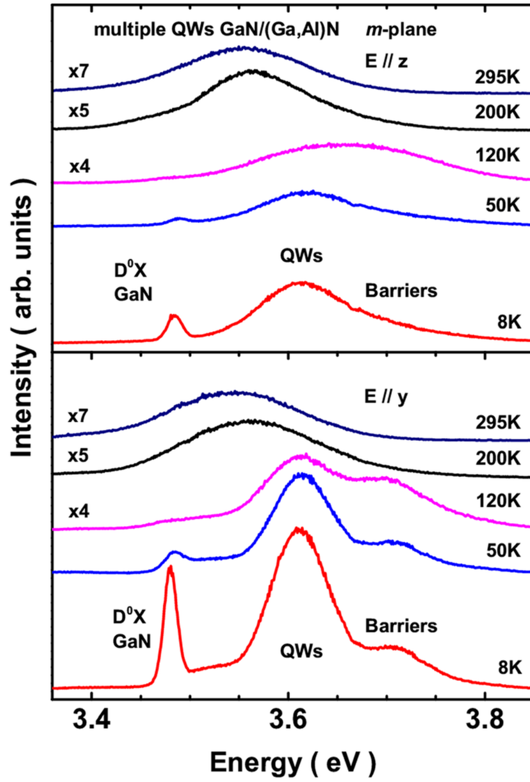

FIG. 6. Plot of the photoluminescence spectra for the *m*-plane grown sample for $\vec{E}//\vec{y}$ (bottom) and $\vec{E}//\vec{z}$ both polarizations (top).

similar behaviors in both polarizations, but the energy is more stable in two cases for the quantum wells when the temperature increases. The photoluminescence energy of the quantum wells is found to be constant up to about 150 K, but that of the barrier layers very slightly blue shifts up to temperatures of about 50 K, above which it collapses rapidly. This is interpreted in terms of the thermal de-trapping of the carriers from aluminum poor regions to aluminum-rich ones. The fit to the data using model by Viña *et al.*[32] (and Eq. (3) of Ref. 33) $E_g(T) = E(0) - \frac{\alpha_B \Theta_B}{\exp(\Theta_B/T)-1}$, indicated an average phonon bath temperature (Θ_B) of 335–340 K for the barrier layers, while 500 K for the multiple quantum wells, for both $\vec{E}//\vec{y}$ and $\vec{E}//\vec{z}$ polarizations. In a sense there is no marked influence of the polarization. At this stage, one would anticipate that the photoluminescence intensity in the MQWs is *influenced by and correlated to* carrier de-trapping in the barrier layers. This argument is supported by the high resolution of the photoluminescence spectra for $\vec{E}//\vec{y}$ polarization compared to spectra corresponding to photons collected with $\vec{E}//\vec{z}$ polarization.

We now wish to calibrate the relative contributions of radiative and non-radiative recombination processes in our sample. The photoluminescence intensity is a quantity that varies proportional with the ratio of non-radiative (τ_{nonrad}) to radiative (τ_{rad}) decay times:

$$\mathrm{I}(T) \propto \frac{\tau_{nonrad}}{\tau_{nonrad} + \tau_{rad}} \propto \frac{1}{1 + \frac{\tau_{rad}}{\tau_{nonrad}}}. \tag{4}$$

The radiative recombination rate *G(T)*, which is the inverse of the radiative decay time is proportional to the relative number of excitons with vector in the light cone (the relative population of excitons with wave vectors smaller than $\frac{E}{\hbar c}$).[34]

$$\mathrm{G}(T) = \frac{1}{2\tau_{rad}} \propto \frac{\int_0^{E/\hbar c} \exp\left(-\frac{\hbar^2 k^2}{2\mathrm{M}(k) k_B T}\right) d^n k}{\int_0^{\infty} \exp\left(-\frac{\hbar^2 k^2}{2\mathrm{M}(k) k_B T}\right) d^n k}, \tag{5}$$

where $d^n k$ is the elemental volume in the n-dimensional k space. This dimension n = 3 for a bulk material, $n = 2$ for a quantum well, $n = 1$ for a quantum wire and $n = 0$ for a zero dimensional sample of a dot or impurity. Here, M(k) is a direction-weighted excitonic translation mass, and the exciton population has been taken to be Maxwellian to allow the use of analytical expressions. Finally, in an n-dimensional integration condition, the radiative decay time can be expressed as:

$$\tau_{rad} = \tau_0 T^{\frac{n}{2}}. \tag{6}$$

The non-radiative decay time is thermally activated and can be written as:

$$\tau_{nonrad} = \tau_1 \exp\left(\frac{E_a}{k_B T}\right) = \tau_1 \exp\left(\frac{T_a}{T}\right) \tag{7}$$

with an activation energy (temperature) E_a (T_a). The larger the E_a (T_a), the higher the value of τ_{nonrad}, providing a better photoluminescence robustness with increasing temperature.

Finally, the variation of the photoluminescence intensity with temperature may be fitted by:

$$I(T) \propto \frac{1}{1 + \frac{\tau_0}{\tau_1} T^{\frac{n}{2}} \times \exp\left(-\frac{T_a}{T}\right)}. \tag{8}$$

In Figure 8, we present the behavior of the photoluminescence intensities for quantum wells and barrier layers in the $\vec{E}//\vec{y}$ and the $\vec{E}//\vec{z}$ polarizations. The photoluminescence

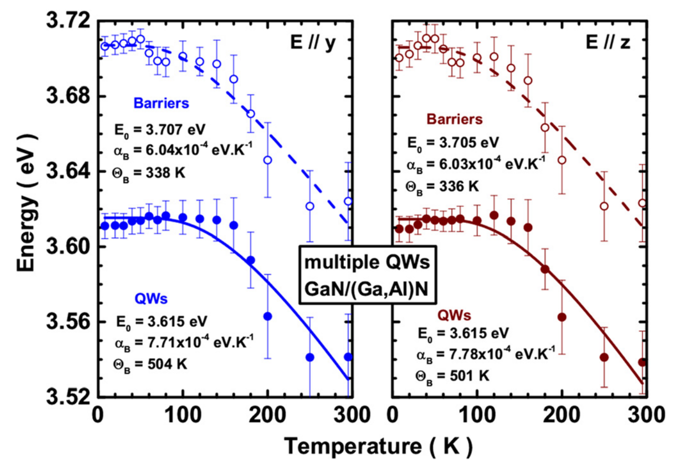

FIG. 7. Plot of the photoluminescence energies for the *m*-plane grown sample for $\vec{E}//\vec{y}$ (left-hand side) and $\vec{E}//\vec{z}$ both polarizations (right-hand side). Photoluminescence energies in the barrier layers and in the quantum wells are both plotted and fitted using Viña's equation.

[This article is copyrighted as indicated in the article. Reuse of AIP content is subject to the terms at: http://scitation.aip.org/termsconditions. Downloaded to] IP: 128.172.48.59 On: Mon, 19 Oct 2015 16:20:56

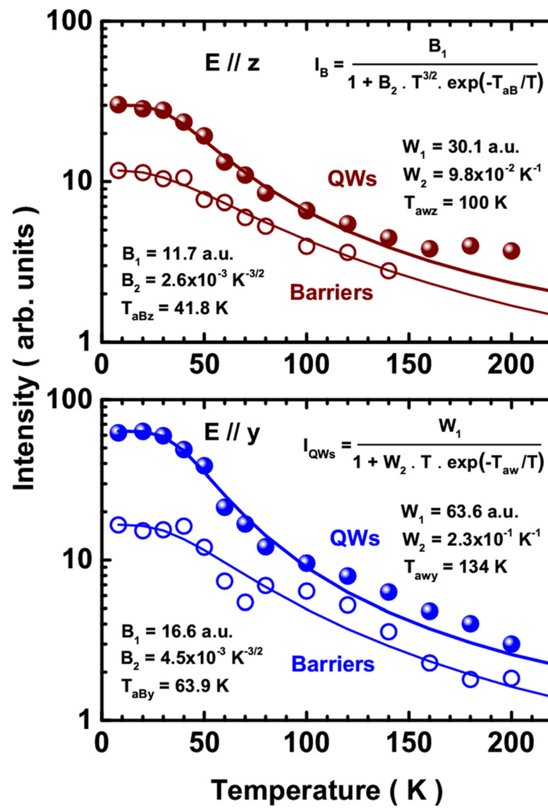

FIG. 8. Plot of the photoluminescence intensities for the *m*-plane grown sample in case of $\vec{E}//\vec{y}$ polarization (bottom) and $\vec{E}//\vec{z}$ polarization (top). The quantum wells related intensities are plotted using full dots while the barrier related data is plotted using open dots. The experimental data are represented using full or open dots while the results of the fitting procedure are reported using continuous lines. The parameters for the fit are indicated in all cases as well as the fitting functions for QWs (bottom plot equation) and the barriers (top plot equation), using W and B letters to represent the parameters of fits.

intensity of the barrier layers were fitted in the framework of a three-dimensional model for propagation of excitons while that for the quantum wells were fitted using a two-dimensional model (this gave the best results and also probes the existence of vertical transport the MQWs). The robustness of both barrier and quantum well-related photoluminescence are better in the $\vec{E}//\vec{y}$ polarization than in the $\vec{E}//\vec{z}$ polarization as indicated by the values of the fitting parameters. The smaller activation temperature for barrier layers than for quantum wells governs the non-radiative recombination. Note that ratios $\frac{\tau_0}{\tau_1}$ are labeled W_2 for well layers and B_2 for barrier layers to distinguish their dimensions. The Arrhenius plot (logarithm of the photoluminescence intensity versus T^{-1}) is a conventional representation and it is given in Figure 9 for the readers' benefit. Inserted in the bottom part of Figure 9, is the experimental and theoretical (line representing the differences of the fits of energies) values of energy splitting between the barrier and the well contributions to the photoluminescence.

V. TIME-RESOLVED PHOTOLUMINESCENCE SPECTROSCOPY

In order to obtain the values of the radiative and non-radiative decay times, we examined the temperature dependent photoluminescence decays. The relationship between the photoluminescence decay time τ, the non-radiative (τ_{nonrad}) and radiative (τ_{rad}) decay times is:

$$\frac{1}{\tau} = \frac{1}{\tau_{rad}} + \frac{1}{\tau_{nonrad}}. \quad (9)$$

Figure 10 illustrates the recombination kinetics of the photoluminescence of the quantum well up to 70 K where a mono-exponential decay is noted.

To extract the radiative and non-radiative decay times one further makes the assumption that non-radiative recombination processes are slower than the radiative ones at low temperature, and normalizes the photoluminescence intensity to unity at low temperature. The radiative and non-radiative decay times obtained as such are provided in Figure 11 together with the measured values of the decay time.

We remark that as the temperature reaches 80 K the decay times saturate in the 50 ps range for the quantum wells in both polarization conditions, while they are more robust for the barrier layers for which the "saturation temperature" is around 150 K. From the evolution of photoluminescence intensity with temperature, we can extract radiative and non-radiative contributions. For the barrier layers, the radiative part increases non-linearly with the temperature and is fitted with $\tau_0 T^{3/2}$ where $\tau_{0y} = 1.6 \times 10^{-1}$ ps.K$^{-3/2}$ for $\vec{E}//\vec{y}$ and $\tau_{0z} = 9.8 \times 10^{-2}$ ps.K$^{-3/2}$ for $\vec{E}//\vec{z}$. The corresponding

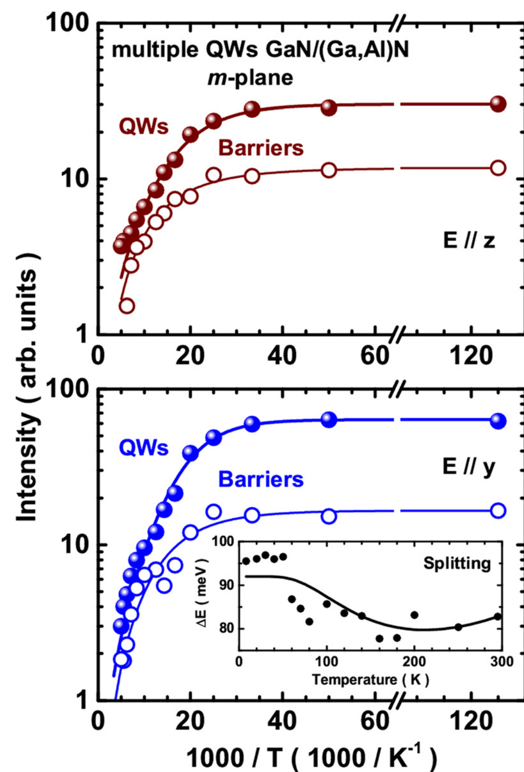

FIG. 9. Arrhenius plots of the photoluminescence intensities for the *m*-plane grown sample in case of both polarizations: $\vec{E}//\vec{y}$ (bottom) and $\vec{E}//\vec{z}$ (top) polarizations. The experimental data are represented with full or open dots while the results of the fitting procedure are reported using continuous lines. The parameters for the fit are given in figure 8. Inserted in the bottom part plot, is the experimental (full dots) and theoretical (line representing the differences of the fits of energies using Viña's model) values of energy splitting between the barrier and the well contributions to the photoluminescence.

[This article is copyrighted as indicated in the article. Reuse of AIP content is subject to the terms at: http://scitation.aip.org/termsconditions. Downloaded to] IP: 128.172.48.59 On: Mon, 19 Oct 2015 16:20:56

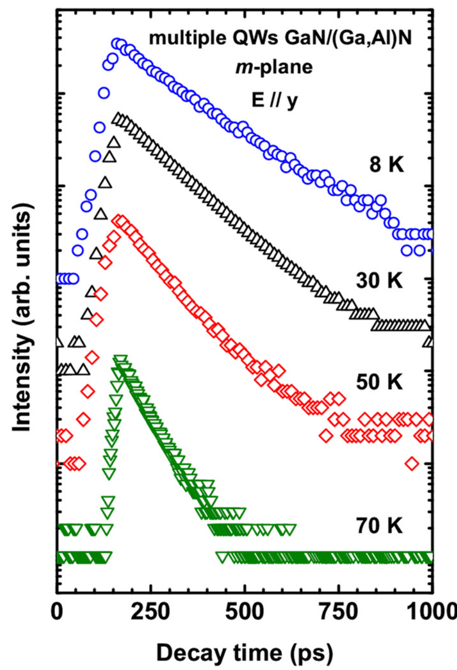

FIG. 10. Typical decays of the photoluminescence of the quantum wells measured for temperature ranging from 8 K up to 70 K.

activation temperatures (T_a) are 64 K and 42 K, respectively, providing $\tau_{1y} = 36\,ps$ and $\tau_{1z} = 38\,ps$.

Regarding quantum wells, a constant value of decay time up to 50–60 K is indicative of localization of the excitons, in agreement with intensity versus temperature data. The excitons become mobile in the quantum well planes and the expected linear dependence with temperature is deduced from the experiments. Values of $\tau_{0y} = 4.7\,\text{ps.K}^{-1}$ and $\tau_{0z} = 3.1\,\text{ps.K}^{-1}$ are proposed here as relevant values.

Regarding the non-radiative components, activation temperatures of $T_a = 134\,\text{K}$ for $\vec{E}//\vec{y}$ and $T_a = 100\,\text{K}$ for $\vec{E}//\vec{z}$ were obtained, which are in agreement with temperature dependence of photoluminescence intensities, giving

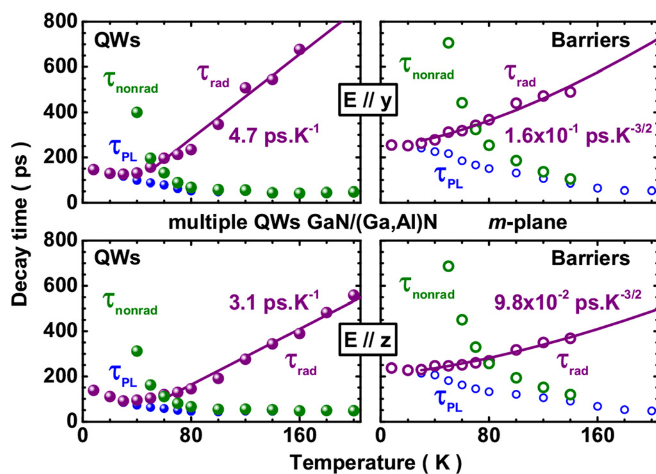

FIG. 11. Recombination decay times (green dots) with non-radiative (bleu dots) and radiative (wine dots) components for the *m*-plane grown sample in case of $\vec{E}//\vec{y}$ (top) and $\vec{E}//\vec{z}$ (bottom) polarizations. The quantum wells data are represented using full dots (left-hand side) and the barriers layers with open dots (right-hand side). The solid lines represent the fit of radiative times data.

$\tau_{1y} = 20\,\text{ps}$ and $\tau_{1z} = 32\,\text{ps}$. We remark that T_a of the quantum wells is higher than that of the barriers layers. We also emphasize that, based on the relative temporal behavior, the recombination dynamics in the quantum wells are ruled by non-radiative recombination at high temperatures and that its decay is ruled by carrier feeding from the barrier layers.

The radiative decay time for quantum wells grown on *m*-plane substrates can be written in the frame work of one valence band as:[35]

$$\tau_{rad}(T) \approx \frac{2c^2 k_B}{\hbar\omega_{LT} a_B{}^3}\left(\frac{1}{m_{ey}+m_{hy}} + \frac{1}{m_{ez}+m_{hz}}\right)^{-1} \frac{\lambda^2}{\omega^3 I_{eh}{}^2} T, \tag{10}$$

where k_B is the Boltzmann constant, c is the velocity of light, a_B is the bulk Bohr radius, ω is the light angular frequency, λ is the in-plane exciton Bohr radius in the quantum well and ω_{LT} is the angular frequency of the longitudinal splitting of the exciton. The radiative decay quantity is directly obtained from a line shape fitting of the photoluminescence of the reflectivity of GaN. The quantity $m_{ei} + m_{hi}$ is the translation exciton mass in the i direction and I_{eh} is the overlap of electron and hole envelope functions. This equation also holds for c-plane quantum wells, in which case $m_{ez} + m_{hz}$ is replaced with $m_{ex} + m_{hx}$. Note that the Quantum Confined Stark Effect is responsible for the strong variations of τ_{rad} with well-width through quantities λ, ω and I_{eh}. We emphasize that, in a given growth orientation, quantity $\frac{\lambda^2}{\omega_{LT}\omega^3 I_{eh}{}^2}$ in Eq. (10) contains all the needed information to determinate the polarization dependence and well-width dependence of the slope of τ_{rad} against temperature.

In regard to different orientations, we have previously obtained $\tau_0 = 20\,\text{ps.K}^{-1}$ and $\tau_0 = 8\,\text{ps.K}^{-1}$ for c-plane[36] and $(11\bar{2}2)$-oriented $GaN/Al_{0.5}Ga_{0.5}N$ quantum wells,[37] respectively, and $\tau_0 = 20\,\text{ps.K}^{-1}$ for homopitaxial *m*-plane ZnO/ZnMgO quantum wells.[35] He we report 4.7 ps.K^{-1} for the $\vec{E}//\vec{y}$ polarization and 3.1 ps.K^{-1} for the $\vec{E}//\vec{z}$ polarization. We believe that these values are in concert with other experimentally measured values (for instance, see Cofdir *et al.*[38]) and are compatible with the predictions of the simple theory and deserve further studies. Obviously, the slope is a little bit smaller than the expected value probably because of the competition between the localized and delocalized excitons through the whole temperature range of this experiment.

VI. CONCLUSIONS

In conclusions, we have reported experimental anisotropy of the in plane optical response for GaN/AlGaN quantum wells grown on *m*-plane GaN substrate. We do not observe the signature of staking faults on basal plane typical of non-polar GaN epilayers grown on lattice mismatched substrates (No PL line at 3.42 eV). The excitonic recombination is dominantly radiative up to 80 K in our moderately shallow quantum wells. At high temperatures it is dominated by non-radiative recombination channels and the thermally induced de-trapping of the carriers photo-created in the

[This article is copyrighted as indicated in the article. Reuse of AIP content is subject to the terms at: http://scitation.aip.org/termsconditions. Downloaded to] IP: 128.172.48.59 On: Mon, 19 Oct 2015 16:20:56

barrier layers influences the recombination dynamics and the robustness of the photoluminescence.

ACKNOWLEDGMENTS

The work at VCU was funded by a Materials World Network grant from the National Science Foundation (DMR-1210282) under the direction of C. Ying. The French group acknowledges support from GANEX (ANR-11-LABX-0014). GANEX belongs to the publicly funded "Investissements d'Avenir" program managed by the French ANR agency. Daniel Rosales acknowledges the Ph.D. grant support of international ANR "GASIOPHE".

[1]S. Yoshida, S. Misawa, and S. Gonda, Appl. Phys. Lett. **42**, 427 (1983).
[2]H. Amano, N. Sawaki, I. Akasaki, and Y. Toyoda, Appl. Phys. Lett. **48**, 353 (1986).
[3]I. Akasaki, H. Amano, Y. Koide, K. Hiramatsu, and N. Sawaki, J. Cryst. Growth **98**, 209 (1989).
[4]S. Nakamura, Jpn. J. Appl. Phys. Pt. 2 Lett. **30**, L1705 (1991).
[5]S. Nakamura, M. Senoh, and T. Mukai, Jpn. J. Appl. Phys. Pt. 2 Lett. **30**, L1708 (1991).
[6]I. Akasaki, H. Amano, H. Murakami, M. Sassa, H. Kato, and K. Manabe, J. Cryst. Growth **128**, 379 (1993).
[7]S. Nakamura, M. Senoh, S. Nagahama, N. Iwasa, T. Yamada, T. Matsushita, H. Kiyoki, and Y. Sugimoto, Jpn. J. Appl. Phys. Pt. 2 Lett. **35**, L74 (1996).
[8]T. Takeuchi, S. Sota, M. Katsuragawa, M. Komori, H. Takeuchi, H. Amano, and I. Akasaki, Jpn. J. Appl. Phys. Pt. 2 Lett. **36**, L382 (1997).
[9]J. S. Im, H. Kollmer, J. Off, A. Sohmer, F. Scholz, and A. Hangleiter, Phys. Rev. B **57**, R9435 (1998).
[10]M. Leroux, N. Grandjean, M. Laugt, J. Massies, B. Gil, P. Lefebvre, and P. Bigenwald, Phys. Rev. B **58**, R13371 (1998).
[11]Y. J. Sun, O. Brandt, S. Cronenberg, S. Dhar, H. T. Grahn, K. H. Ploog, P. Waltereit, and J. S. Speck, Phys. Rev. B **67**, 041306(R) (2003).
[12]T. Onuma, A. Chakraborty, B. A. Haskell, S. Keller, S. P. DenBaars, J. S. Speck, S. Nakamura, U. K. Mishra, T. Sota, and S. F. Chichibu, Appl. Phys. Lett. **86**, 151918 (2005).
[13]P. P. Paskov, R. Schifano, T. Malinauska, T. Paskova, J. P. Bergman, B. Monemar, S. Figge, D. Hommel, B. A. Haskell, P. T. Fini, J. S. Speck, and S. Nakamura, Phys. Status Solidi C **3**, 1499 (2006).
[14]S. Okur, K. Jarašiūnas, S. Hafiz, J. Leach, T. Paskova, V. Avrutin, H. Morkoç, and Ü. Özgür, Proc. SPIE **8625**, 86252D (2013).
[15]P. Corfdir, J. Levrat, A. Dussaigne, P. Lefebvre, H. Teisseyre, I. Grzegory, T. Suski, J.-D. Ganiere, N. Grandjean, and B. Deveaud-Pledran, Phys. Rev. B **83**, 245326 (2011).
[16]H. M. Ng, Appl. Phys. Lett. **80**, 4369 (2002).
[17]T. Paskova, V. Drakchieva, P. Paskov, J. Birch, E. Valcheva, P. O. Persson, B. Arnaudov, S. Tugnasmitta, and B. Monemar, J. Cryst. Growth **281**, 55 (2005).
[18]Y. Honda, N. Kameshiro, M. Yamaguchi, and N. Sawaki, J. Cryst. Growth **242**, 82 (2002).
[19]*Nitrides with Nonpolar Surface: Growth, Properties and Devices*, edited by T. Paskova (Wiley-VCH, Weinheim, 2008).
[20]V. Avrutin, G. Cantwell, J. Zhang, J. J. Song, D. Silversmith, and H. Morkoç, Proc. IEEE **98**, 1269 (2010).
[21]R. Mata, A. Cros, J. A. Budagosky, A. Molina-Sanchez, N. Garro, A. García-Cristóbal, J. Renard, S. Founta, B. Gayral, E. Bellet-Amalric, C. Bougerol, and B. Daudin, Phys. Rev. B **82**, 125405 (2010).
[22]S. Schulz, T. J. Badcock, M. A. Moram, P. Dawson, M. J. Kappers, C. J. Humphreys, and E. P. O'Reilly, Phys. Rev. B **82**, 125318 (2010).
[23]M. Funato, K. Matsuda, R. G. Banal, R. Ishii, and Y. Kawakami, Phys. Rev. B **87**, 041306(R) (2013).
[24]R. Liu, A. Bell, F. A. Ponce, C. Q. Chen, J. W. Yang, and M. A. Khan, Appl. Phys. Lett. **86**, 021908 (2005).
[25]T. J. Ochalski, B. Gil, P. Lefebvre, N. Grandjean, J. Massies, and M. Leroux, Solid State Commun. **109**, 567 (1999).
[26]T. J. Ochalski, B. Gil, P. Lefebvre, N. Grandjean, M. Leroux, J. Massies, S. Nakamura, and H. Morkoç, Appl. Phys. Lett. **74**, 3353 (1999).
[27]Here we utilize the notations of the excitonic symmetry in case of orthorhombic crystalline environment. B. Gil and A. Alemu, Phys. Rev. B **56**, 12446 (1997).
[28]S.-H. Park and S.-L. Chuang, Phys. Rev. B **59**, 4725 (1999).
[29]B. Gil, O. Briot, and R. L. Aulombard, Phys. Rev. B **52**, R17028 (1995).
[30]P. Rinke, M. Winkelnkemper, A. Qteish, D. Bimberg, J. Neugebauer, and M. D. Scaeffler, Phys. Rev. B **77**, 075202 (2008).
[31]S.-H. Park, Appl. Phys. A **91**, 361 (2008).
[32]L. Viña, S. Logothetidis, and M. Cardona, Phys. Rev. B **30**, 1979 (1984).
[33]R. Pässler, J. Appl. Phys. **90**, 3956 (2001).
[34]L. C. Andreani, in *Confined Electrons and Photons*, edited by E. Burstein and C. Weisbuch, NATO ASI Series (Plenum Press, New York and London, 1995), Vol. 340, pp. 57–112.
[35]L. Béaur, T. Bretagnon, B. Gil, A. Kavokin, T. Guillet, C. Brimont, D. Tainoff, M. Teisseire, and J.-M. Chauveau, Phys. Rev. B **84**, 165312 (2011).
[36]P. Lefebvre, J. Allegre, B. Gil, A. Kavokine, H. Mathieu, H. Morkoç, W. Kim, A. Salvador, and A. Botchkarev, Phys. Rev. B **57**, R9447 (1998).
[37]D. Rosales, T. Bretagnon, and B. Gil, Phys. Rev. B **88**, 125437 (2013).
[38]P. Corfdir, A. Dussaigne, H. Teysseire, T. Suski, I. Grzegory, P. Lefebvre, E. Giraud, M. Shahmohammadi, R. T. Philips, J. D. Ganière, N. Grandjean, and B. Deveaud, Jpn. J. Appl. Phys., Part 1 **52**, 08JC01 (2013).

[This article is copyrighted as indicated in the article. Reuse of AIP content is subject to the terms at: http://scitation.aip.org/termsconditions. Downloaded to] IP: 128.172.48.59 On: Mon, 19 Oct 2015 16:20:56